About drivers of performance for crop growth model calibration at the within-field scale

Daniel Pasquel, James A Taylor, Bruno Tisseyre, Sébastien Roux

European Journal of Agronomy 170 (2025) 127773

Contents lists available at ScienceDirect

European Journal of Agronomy

journal homepage: www.elsevier.com/locate/eja

About drivers of performance for crop growth model calibration at the within-field scale

Daniel Pasquel [a,b,*], James A. Taylor [a], Bruno Tisseyre [a], Sébastien Roux [c]

[a] ITAP, Univ. Montpellier, INRAE, Institut Agro, Montpellier, France
[b] EMMAH, INRAE, Avignon Université, Avignon, France
[c] MISTEA, Univ. Montpellier, INRAE, Institut Agro, Montpellier, France

ARTICLE INFO

Keywords:
Predawn leaf water potential
WaLIS
Spatial calibration
Precision agriculture
Spatial pattern

ABSTRACT

The calibration process is a necessary step to improve crop growth model (CGM) performances and to reduce the uncertainty related to model parameters. Modeling agronomic variables at the within-field scale needs to accurately reproduce the spatial pattern to enable a suitable spatial management. Spatial calibration is one efficient downscaling method for CGM spatialization. The objective of this study is to better understand the drivers of performance of spatial calibration by comparing it to an aspatial calibration (i.e. at field or site-specific scale) in various conditions. The impact of three driving properties was studied: the targeted variable variance, its level of spatial structure, and the correlation level of ancillary data. To this aim, a method was designed to simulate various spatial structures from the one of an existing vineyard whilst ensuring the temporal consistency of the simulated data. The method was applied to a vineyard CGM (WaLIS) aiming at estimating plant water restriction using predawn leaf water potential (Ψ_{PD}) measurements. Results showed that spatial calibration improved the model performances at the within-field scale when Ψ_{PD} was strongly structured and highly correlated to the ancillary data. When Ψ_{PD} was either moderately or weakly spatially structured, the spatial constraint added more error instead of correcting errors, deteriorating the CGM performances. The ancillary data and the segmentation algorithm had a large impact on the spatial calibration performances.

1. Introduction

Crop growth models (CGM) are useful tools for predicting agronomic variables and interactions along the soil-plant-atmosphere continuum. CGM often require a huge number of parameters for their functioning that may involve unmeasurable values or values with large domains of uncertainty in their parametrization (Liu et al., 2018a). These uncertainties affect CGM outputs and thus reduce modeling performances (Wallach, 2011; Wallach et al., 2014). Improve the reliability of CGM is of primary interest and is mainly based on the way to parametrize models, it allows to reduce the sources of uncertainty (Wallach et al., 2016). The sources of uncertainty in predicting agronomic variables are well known and are based on (i) the model structure, (ii) the input data and (iii) the model parameters (van Oijen and Ewert, 1999). Seidel et al. (2018) highlighted that calibration process to parametrize CGM is an important source of uncertainty with still a potentiality to be improved.

In a precision agriculture (PA) context, CGM could be used to identify the most relevant management strategy to be applied at the within-field scale. However, applying a CGM at the within-field scale involves using a model spatialization approach to adjust the native spatial footprint of the model to a finer-scale prediction of agronomic variables (Pasquel et al., 2022). Spatial calibration approaches can play a valuable role in modifying the spatial footprint of CGM as part of the spatialization process. In the case of prediction with CGM at the within-field scale, calibration of model parameters is performed to adjust for local site-specific variability without changing the model equations. In other words, spatial calibration approaches aims to spatialize CGM without modifying their point-based simulation formalisms. Modifying their formalisms could result in spatial GCM, but such models are out of the scope of this study.

Batchelor et al. (2002) presented various strategies for spatially applying CGM at the within-field scale, emphasizing the importance of applying CGM to homogeneous zones and the need to accurately define these zones. CGM can be applied spatially at within-field scale by employing either a point-based approach on a regular grid (Irmak et al., 2001; Wallor et al., 2018) or at specific measurement sites where

* Corresponding author at: EMMAH, INRAE, Avignon Université, Avignon, France.
E-mail address: daniel.pasquel@inrae.fr (D. Pasquel).

https://doi.org/10.1016/j.eja.2025.127773
Received 20 December 2024; Received in revised form 27 May 2025; Accepted 12 July 2025
Available online 17 July 2025

observed data are available for calibration (Pasquel et al., 2023). Both approaches, often referred to as site-specific modeling, represents the finest resolution for CGM application based on available data. Another approach involves spatially constraining the calibration process, aligning this later with within-field management zones and/or spatial characteristics of agronomic variables. Within-field zone delineation is common in PA (Corwin and Lesch, 2005; Tagarakis et al., 2018). Applying CGM on these defined within-field zones ensures spatial consistency in simulating agronomic variables (Thompson et al., 2024; Thorp et al., 2008). These homogeneous zones can also be delineated using ancillary data that capture spatial variability, such as soil properties or NDVI (Acevedo-Opazo et al., 2008; Bahat et al., 2024; Cammarano et al., 2021; Gaso et al., 2021; Leo et al., 2023; Maestrini and Basso, 2018; Ziliani et al., 2022).

An assumption behind this existing method is that constraining the spatial pattern of the agronomic variable will allow a spatially consistent smoothing of the calibration error relative to the measured data set. However, such data are either rarely available or may present a high level of noise to carry a calibration at a finer spatial scale. Thus, it is not immediately apparent if a calibration at a finer spatial scale will be able to efficiently reproduce the spatial pattern of the target agronomic variable. However, the effectiveness and achievable spatial resolution of such spatial calibration approach have not been extensively investigated. Comparison between site-specific scale, within-field zone and field scale has been rarely carried out (He et al., 2024; Trenz et al., 2024). Moreover, three potential drivers have a questionable impact on the spatial calibration process:

(i) the degree of the spatial structure/pattern of the agronomic variable to be predicted;

(ii) the total variance of the agronomic variable to be predicted;

(iii) the degree of correlation between the agronomic variable to be predicted and the ancillary data used to delineate within-field calibration zones.

Understanding their role can be a practical issue in order to predict performance of spatial calibration, but no such study has been carried out so far, probably because studying the effect of spatial structure requires many experimental data covering many spatial structures.

The objective of this study is to investigate how relevant it is to spatialize CGM by using spatial calibration for using a CGM at the within-field scale and in particular to identify in which situations the use of a spatial calibration is better than an aspatial calibration (i.e. at field or site-specific scale). To overcome the lack of data needed to understand the sensitivity of the spatial calibration performance to the three drivers, an original hybrid approach using spatial perturbations of experimental data was specifically designed. This approach was applied to the CGM named WaLIS (Celette et al., 2010) which is designed to simulate predawn leaf water potential (Ψ_{PD}) of vine during growing season (with the intention of managing water stress) and using real Ψ_{PD} measurements.

2. Material and methods

2.1. Field data

The experimental vineyard used for this study was a 1.2 ha Syrah non-irrigated vineyard located in the south of France (43.144°N, 3.131°E, Gruissan, Aude) on the INRAE Pech Rouge experimental site. Spacing between each vines measure 1 m and between each row measure 2.5 m. The vineyard is cultivated on a limestone plateau and is characterized with clay accumulation at some locations impacting the soil spatial heterogeneity. The agronomic variable of interest was the predawn leaf water potential (Ψ_{PD}) representative of the vine water stress. Ψ_{PD} was manually measured for two consecutive years (2003 and 2004) on several dates (respectively 7 and 2 dates) at the within-field scale on 49 measurement sites using a pressure chamber (more details are available in Acevedo-Opazo et al. 2010 for this data set) (Fig. 1).

2.2. WaLIS and the predicted predawn leaf water potential (ΨPD)

The crop model Water baLance for Intercropped Systems – WaLIS, (Celette et al., 2010) was used to predict the Ψ_{PD}. WaLIS is not exactly a CGM but a hydric model related to vine physiology, but it presents the same structure and the same characteristics than a CGM, reason why WaLIS was chosen. The main output of WaLIS is the vine water status represented by the Ψ_{PD} and it has only few inputs, i.e. the weather data, the soil characterization and few parameter related to the vine physiology. The 2003 and 2004 weather data acquired through the weather station 11170004 (Gruissan) of the INRAE network at nearly 350 m of the experimental vineyard were used as WaLIS input data (Fig. 2). These weather data were collected via the INRAE CLIMATIK platform (Delannoy et al., 2022). They included the daily mean temperature (T_{mean}), the daily precipitation (P) and daily evapotranspiration (ET). ET was computed using the Penman-Monteith equation (Allen et al., 1989; Pereira et al., 1999), for that purpose daily solar radiation, daily relative

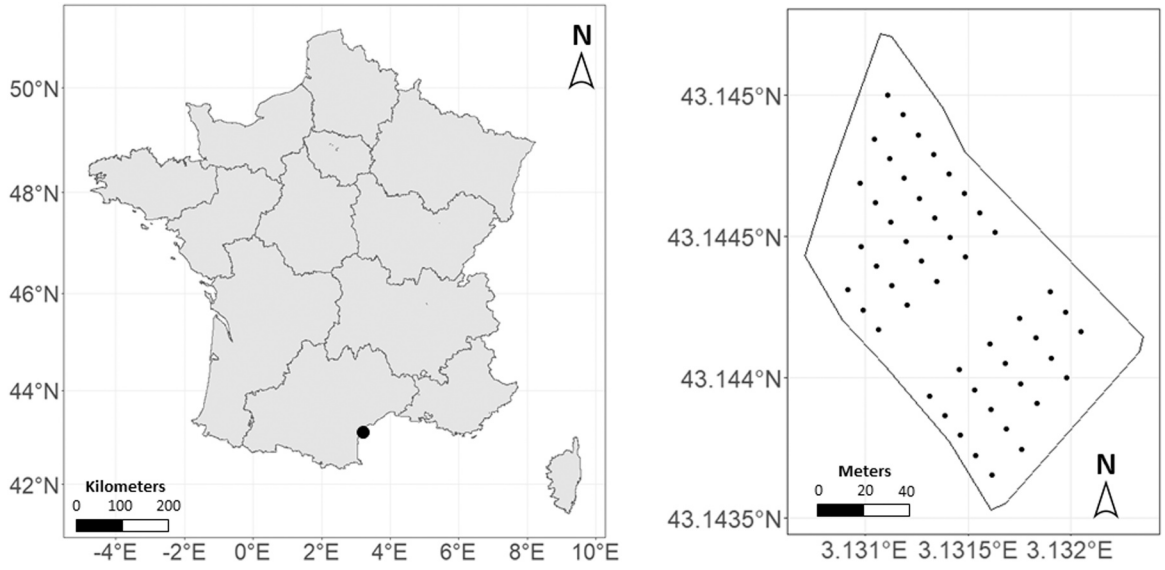

Fig. 1. Location of the experimental Syrah vineyard at INRAE Pech Rouge (Gruissan, Aude, France) (left) and the distribution of the 49 sampling points within the vineyard, where each point represents the location of measured predawn leaf water potential (Ψ_{PD}) on multiple dates during the season.

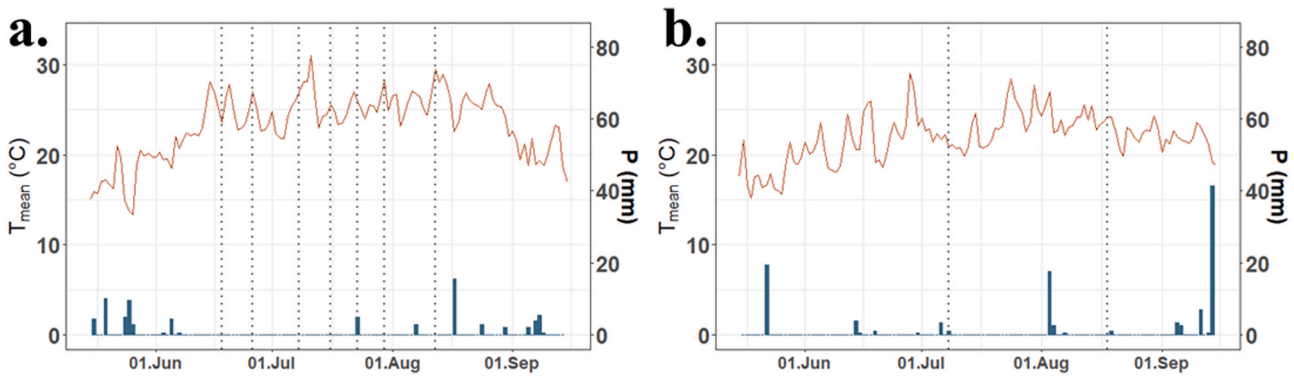

Fig. 2. Weather conditions for the production season for (a.) 2003 and (b.) 2004 with the red line and the blue bars corresponding respectively to the mean temperature (T_{mean}) and the daily precipitation (P). The dashed gray lines correspond to the dates of measurement of Ψ_{PD} considered for this study in 2003 (June 18th, June 26th, July 8th, July 16th, July 23rd, July 30th and August 12th) and 2004 (July 8th and August 18th).

humidity and the daily saturation vapor pressure were also recorded. WaLIS actually simulates the fraction of transpirable soil water (FTSW). Thus, Ψ_{PD} were computed using predicted FTSW following Eq. 1 (refer to Lebon et al., 2003 for further details). Therefore, a relevant and realistic Ψ_{PD} minimum had to be defined because this conversion contained a logarithmic expression and the resulting FTSW value could be equal to 0. This minimum was assumed to the lowest value observed within the 2003–2004 dataset, which was −1.1 MPa. Measured dates in 2003 were used to calibrate WaLIS. The prediction of Ψ_{PD} was carried out in 2004 focusing primarily on the two measurement dates where the water stress in the vineyard was showing a high heterogeneity.

$$\psi_{PD.\mathrm{mod}} = \frac{\log(FTSW) - \log(C_a)}{C_b} \quad (1)$$

where C_a is a constant equal to 1.0572 and C_b is a constant equal to 5.3452 (from Lebon et al., 2003).

2.3. Data generation

2.3.1. Spatially rearranged field simulation

To investigate the impact of various spatial characteristics of vineyard management, simulated data was generated, allowing for accurate control over these characteristics. Thus, spatially rearranged fields (SRFs) were generated. These SRFs are defined in this study as simulated data obtained by spatially rearranging existing data, i.e. forming new simulated vineyards.

They were derived from the available 2004 observed data and their characteristics were constrained by the measurement dates in 2004, regarding their spatial structure of Ψ_{PD} (SS_Ψ) and their total variance of Ψ_{PD} (σ_Ψ). Characteristic of both available dates of measurements (July 8th 2004 and August 18th 2004) are detailed in Table 1. Note that in the followings, resulting simulated vineyards from July 8th 2004 and August 18th 2004 will respectively be referred as low σ_Ψ and high σ_Ψ. For these two measurement dates, the geographic locations of the sampling points were retained but the observed values were redistributed to different sampling points to achieve different spatial structures and patterns. However, each measurement site kept its own temporal profile of Ψ_{PD} using the 2003 dataset, i.e. the temporal profile of the seven measurement dates for 2003, in aim to relevantly calibrate WaLIS. Indeed, in non-irrigated vineyards, the spatial pattern of Ψ_{PD} is known to show a temporal consistency over time as water stress increases (Acevedo-Opazo et al., 2010). In order to carry the spatial rearrangement of the measured sites, changes in Ψ_{PD} values at neighboring locations were considered independent. However, by defining different levels of spatial structures for the spatially rearranged Ψ_{PD}, we introduced intentionally varying degrees of spatial correlation in this study – a factor that we specifically aimed to evaluate in relation to spatial calibration.

Table 1
Characteristics of the predawn leaf water potential (Ψ_{PD}) measured for possible evaluation dates related to their variability and spatial structure. The dates in bold correspond to the considered dates kept for the study having desired coupled characteristics. σ_Ψ = standard deviation of Ψ_{PD} (characterizing the variability), $C_{i.\Psi}$ = Cambardella index of Ψ_{PD} (summarizing the variance spatially organized and the spatial structure).

Date	σ_Ψ (MPa)	σ_Ψ characterization	$C_{i.\Psi}$ (%)	$C_{i.\Psi}$ characterization
08.07.2004	0.10	Low	51	moderate
18.08.2004	0.16	High	32	moderate

Three different modalities to characterize the SS_Ψ were chosen based on the Cambardella index (C_i) (Cambardella et al., 1994). Thus, strong (S) ($C_i < 20$ %), moderate (M) (40 % $< C_i <$ 60 %) and weak (W) (80 % $< C_i$) SS_Ψ were considered. To model the different SS_Ψ, a reference spatial structure with known parameters was simulated using a theoretical variable. This theoretical variable was generated using Gaussian random fields (GRFs) on theoretical fields of size 500 × 500 pixels to ensure the targeted spatial structures were achieved and that the theoretical variogram approximated the experimental variogram (Fig. 3). These 500 × 500 GRFs were created because generated targeted SS_Ψ is easier on larger number of units. Here, the size of each pixel was not a considered variable. The objective was to match both theoretical and experimental variograms to ensure the targeted spatial structures properties. Thus, the overall size of the GRF (500 × 500 pixels) was carefully chosen to meet this objective. Then, new 49-unit GRFs were generated (corresponding to the 49 initial measurement sites), with the same field shape as the real vineyard field (Fig. 3). These new GRFs were selected to approximate the targeted spatial structure (i.e. defined by the 500 × 500 GRFs) to ensure the spatial structure characteristic conservation of each considered SS_Ψ modalities (S, M and W). Every spatial structure was estimated by theoretical variograms fitted with a REML method, more suitable when limited data are available to compute variograms (Kerry and Oliver, 2007). Thus, when both theoretical variograms of targeted GRFs and 49-unit GRFs were close (i.e. with a similar C_i and a weak RMSE computed between each lag), spatial structures were assumed to be similar, i.e. the generated 49-unit GRFs were considered to have the desired SS_Ψ modality and the considered 49-unit GRF was kept (Fig. 3). Then, the same approach was used to reassign the Ψ_{PD} values from the 2004 dataset (Fig. 4) to the 49-unit GRFs. Reassignments were based on value ranking between the 49-unit GRF and the real 49 measurement sites. This reassignment ensured that the spatial structure/pattern characteristics were kept by sorting the values and attributing them according to their rank, i.e. real 49 measurement sites values were orderly reassigned to the 49-unit GRF

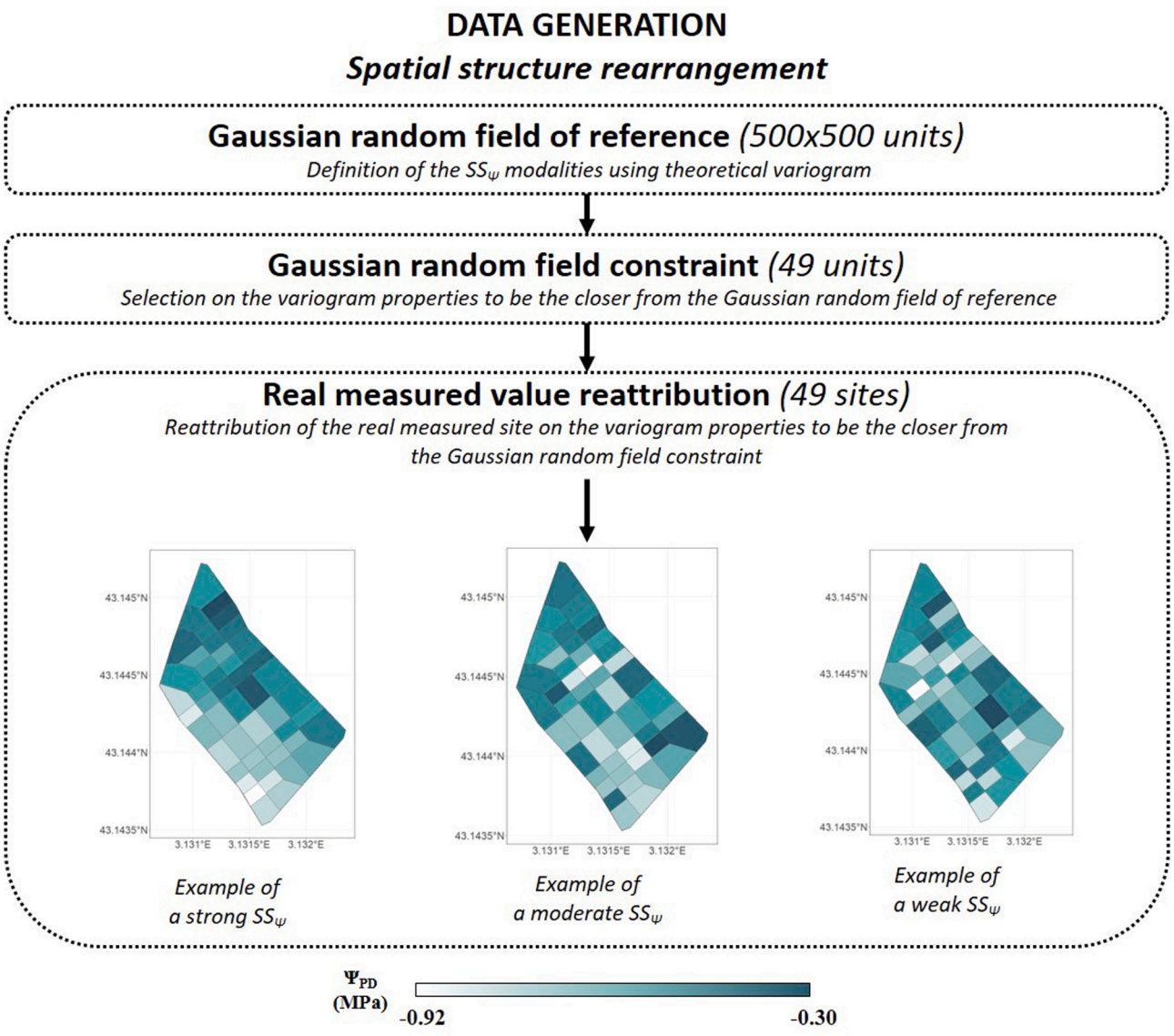

Fig. 3. Data generation by rearranging the real measured sites to match with the targeted spatial structure corresponding to three spatial structure modalities. One example of each spatial structure modalities is illustrated with the rearrangement of the real measured sites. On each map, Voronoi tessellation was used to convert each of the 49 measurement sites of Ψ_{PD} into polygons.

values (this method aimed to conserve a similar spatial structure). Finally, there was 120 SRFs simulated (40 per SS_{Ψ}).

2.3.2. Ancillary data simulation

Ancillary data were also simulated for each generated SRF at three different levels of correlation with the corresponding Ψ_{PD} (ϱ_{AD}) at the evaluation dates. As a result, these ancillary data were spatially correlated with the SRF. For the record, it is very common to consider ancillary data in a PA context. Ancillary data are usually easier to get and are used to give information on the spatial structure/pattern of the considered agronomic variable (e.g. variables related to vine vigor, soil properties). Simulating auxiliary data thus allows the implementation of this common reasoning in PA while controlling ϱ_{AD}. These simulated ancillary data were the only data used to delineate within-field zones. To be able to modify ϱ_{AD}, the method from Oger et al. (2021) was adapted to simulate the ancillary data as needed for this study (Eqs. 2 and 3).

$$AD_i = \psi_{PD_i} + \varepsilon_{iwith\varepsilon_i N(0,\sigma_{AD}{}^2)} \quad (2)$$

$$\sigma_{AD}{}^2 = \frac{\sigma_{\psi}{}^2}{(Cor(\psi_{PD}, AD))^2} - \sigma_{\psi}{}^2 with\ Cor(\psi_{PD}, AD)\epsilon[0,1] \quad (3)$$

where AD_i is the ancillary data value at the location i, ψ_{PD_i} is the Ψ_{PD} value at the location i, $\sigma_{AD}{}^2$ is the variance of simulated ancillary data, $\sigma_{\psi}{}^2$ is the variance of predawn leaf water potential reassigned and $Cor(\Psi_{PD},AD)$ is the Pearson correlation between both variables.

In other words, with the assumption of second-order stationarity, the variance of Ψ_{PD} and ancillary data corresponded to the sill values of the theoretical variogram. Thus, depending on the expected ϱ_{AD}, the variance to be added to the Ψ_{PD} values was determined by Eq. 2. The correlation levels considered were 94 %, 50 % and 10 % for ϱ_{AD} within the SRFs. These three levels were selected based on correlations observed in the literature between normalized difference vegetation index and vine physiology parameters (Bramley et al., 2019; Hall et al., 2011) and to provide strongly contrasting levels.

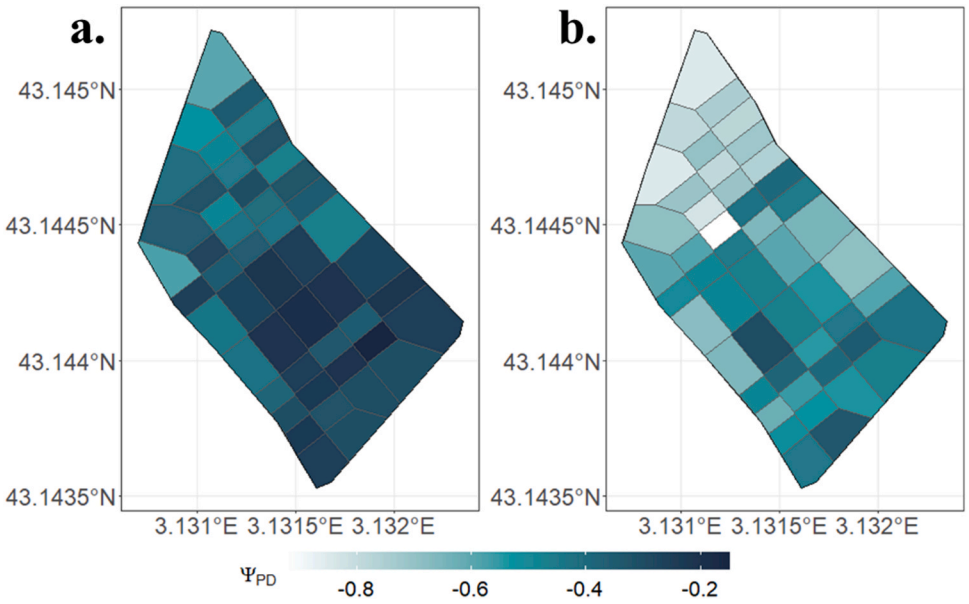

Fig. 4. Predawn leaf water potential (Ψ_{PD}) measured on the experimental vineyard on (a.) July 8th 2004 corresponding to the date with low total variance of Ψ_{PD} (σ_Ψ) and (b.) August 18th 2004 corresponding to the date with high σ_Ψ. Voronoi tessellation was used to convert each of the 49 measurement sites of Ψ_{PD} into polygons.

2.4. Calibration approaches

2.4.1. Spatial calibration

The spatial calibration was defined as a calibration process based on the delineation of calibration zones from ancillary data that were representative of the spatial pattern of the considered agronomic variable. For further details about the spatial calibration approach please refer to Pasquel et al., (2023)). In that case, using spatial calibration implies applying a spatial constraint to the calibration process, driven by the use of within-field zones derived from a segmentation algorithm applied to spatial ancillary data.

Step 1: Parameter possibly spatially heterogeneous at within-field scale identification

The WaLIS parameters identified as likely to have some spatial variation were the total transpirable soil water (TTSW) and the maximum crop coefficient of the vine (K_C) (McClymont et al., 2019; Verdugo-Vásquez et al., 2022). Note that in Celette et al. (2010) as there is 2 different crops, the authors chose to use K_V and K_{IC} respectively for crop coefficient of the grapevine and crop coefficient of the intercrop, here as only vine is considered, K_C was used as generic term. Other WaLIS parameters were aspatially defined and their values were kept constant at a level representative of the environmental context from where the original data were measured (Celette et al., 2010). The TTSW and K_C were spatially calibrated by finding the optimal parameter values on a 2-dimension grid using the measured data from Ψ_{PD} 2003. The TTSW values ranged from 55 to 210 mm in increments of 5 mm and the K_C values ranged from 0.35 to 0.5 in increments of 0.05, i.e. represent the possible parameter couple of TTSW and K_C for the model calibration. These domain ranges were defined regarding expert knowledge and represent the diversity of cases which are possible to meet in the original environmental context (Roux et al., 2019). Calibrated values were those that minimized the mean absolute error (MAE) compared to all Ψ_{PD} measurements realized in 2003.

Step 2: Delineation of the calibration zones

Within-field zones were delineated using a segmentation algorithm (Pedroso et al., 2010) included in the *GeoFIS* R package (Guillaume and Lablée, 2022) applied to the simulated ancillary data for each generated SRF. The considered number of within-field zones were between 2 and 5 zones. This number of within-field zone has been chosen because it could be representative of a realistic management clustering in PA.

Step 3: Selection of the best within-field spatial modeling scale

Concerning the ϱ_{AD}, the hypothesis was that the higher the level of correlation of the ancillary data with the Ψ_{PD}, the more relevant the delineation will be. Thus, the relevance of the delineation was evaluated by a one-way analysis of variance (ANOVA) linking Ψ_{PD} with the delineated zones. The more the delineation explained the variation in Ψ_{PD}, the more the delineation was considered relevant. Therefore, SRFs were kept depending on the delineation relevance, i.e. based on the proportion of variability explained by the delineated within-field zones. After the delineation of the calibration zones, the mean value of the measured sites within each zone was used for the spatial calibration, i.e. the modeling was performed at the spatial scale of the zones.

2.4.2. Aspatial calibration

The aspatial calibration approach was based directly on the simulated vineyards and applied at two scales, i.e. at field and at the site-specific scales. Calibration at field scale was performed on an aspatial calibration using field averages (i.e. average of all measurement points), which is the supposed original spatial footprint of CGM (Pasquel et al., 2022). Calibration at site-specific scale was performed on an aspatial calibration where each point was individually calibrated. This resulted in crop model outputs at either the field or the site-specific scale. The calibration at the site-specific scale is not considered as spatial calibration because each site is individually calibrated from the others. Thus, individually, each site-specific area corresponds to 0.25 ha.

2.5. Modeling performance evaluation

Crop model outputs resulting from both aspatial and spatial calibration approaches were compared to estimate which calibration approach was the most relevant. Thus, outputs of the spatial calibration approach were compared to the outputs of the aspatial calibration approach corresponding to the site-specific scale modeling and the field scale modeling. For all the modeling, outputs were disaggregated to the site-specific scale to assess the relevance of the spatial calibration. To evaluate outputs of spatialized WaLIS, the root mean square error (RMSE) (Eq. 4) and the spatial balanced accuracy (SBA) (Eq. 5) (Pasquel et al., 2023) were used. The SBA score was used to account for the

preservation of the spatial pattern of the outputs. It provides an assessment of both aspatial and spatial pattern errors. Thus, SBA was used on each spatial modeling scale.

$$RMSE = \sqrt{\frac{1}{n}\sum_{i=1}^{n}(O_i - M_i)^2} \quad (4)$$

where O_i is the observed Ψ_{PD}, M_i is the corresponding modeled Ψ_{PD} and n is the number of observation (n = 49).

$$SBA(O,M) = \frac{1}{100}\sum_{q=1}^{100}\left[1 - BA\left(O_{t(O,M,q)}, M_{t(O,M,q)}\right)\right] \quad (5)$$

where O and M are respectively the observed and modeled maps, $O_{t(O,M,q)}$ and $M_{t(O,M,q)}$ are respectively the observed and modeled maps at the threshold level $t(O,M,q)$ corresponding to percentile q on the merging data distributions of O and M.

The SBA score was used to determine the optimal scale for spatial calibration, specifi-cally within-field zonal scales. For each simulated vineyard, the best-performing spatial scale (n-zones) was identified and compared to aspatial calibration approaches at both the field and site-specific scales. Since the SBA score is designed to compare spatial modeling within the same field (Pasquel et al., 2023), the difference in SBA score (ΔSBA) was calculated to enable comparisons across different SRFs. The ΔSBA evaluated the effectiveness of spatial calibration by comparing it to aspatial calibration at the site-specific scale (ΔSBA_{site}) (Eq. 6) or the field scale (ΔSBA_{field}) (Eq. 7). A positive ΔSBA indicated that spatial calibration performed better, i.e. producing results with closer numerical values and spatial patterns, while a negative ΔSBA indicated better performance by the aspatial approach.

$$\Delta SBA_{site} = SBA(O, M_{site}) - \min_{zone\in\ \{2,3,4,5\}}\left[(SBA(O, M_{zone})\right] \quad (6)$$

where M_{site} is the Ψ_{PD} modeled using an aspatial calibration approach at the site-specific scale and M_{zone} is the Ψ_{PD} modeled using a spatial calibration approach for each considered within-field zones.

$$\Delta SBA_{field} = SBA(O, M_{field}) - \min_{zone\in\ \{2,3,4,5\}}\left[(SBA(O, M_{zone})\right] \quad (7)$$

where M_{field} is the Ψ_{PD} modeled using an aspatial calibration approach at the field scale and M_{zone} is the Ψ_{PD} modeled using a spatial calibration approach for each considered within-field zones.

2.6. Statistical analysis

As the computational time was relatively high, 120 simulated vineyards were generated to have simulation within an acceptable computational power. Considering the 3 modalities of ϱ_{AD}, the selected best within-field spatial modeling scale and the aspatial calibration scales (i.e. field and site-specific scale), there were 1080 simulations for the whole study. All statistical analysis were performed using the R software (R Core Team, 2023). Multiple-way ANOVA was used to evaluate the significance of SS_Ψ, σ_Ψ and ϱ_{AD} in the determination of ΔSBA. Before applying ANOVA, residual normality and homoscedasticity were tested using the Shapiro test and the Levene test respectively. A *post hoc* test, realized using a Tukey's Honest Significant Difference, was used to identify significant pairwise differences among the modalities and to identify which groups were different from the others.

3. Results

First results are about the performances of WaLIS to simulate Ψ_{PD} at different spatial scales. The second part of the results highlights with which combination of the considered drivers the spatial calibration improves the model predictions.

3.1. Performance of WaLIS in predicting Ψ_{PD}

WaLIS performances were similar for both modeling dates (high and low σ_Ψ). For the date with high σ_Ψ, the mean of the different RMSEs obtained for each spatial modeling scale and each ϱ_{AD}, was equal to 0.16 MPa (Fig. 5). Thus, this corresponds to a relative error in predicting Ψ_{PD} (for high σ_Ψ) of 35 %.

For the field scale modeling (i.e. using aspatial calibration), RMSEs were always equal to the average of all the measurement sites and is the same for all the simulated vineyards (Fig. 5b). Similarly, considering the site-scale modeling (i.e. using aspatial calibration), RMSEs were always equal regardless of the spatial arrangement of the measurement sites as the sites values are provided by the 2003 dataset. Indeed, only the measurement site locations were different between each of the simulated vineyards (modification of the SS_Ψ) (Fig. 5b).

The spatialized WaLIS performances were dependent on the delineation level (only the results for the 2 and 5 within-field zones are shown in Fig. 5c) and the correlation between the ancillary data and the Ψ_{PD} (refer to the Supplementary Fig. S.1, S.2 and S.3 to see the WaLIS performances for each level of delineation and each level of correlation for the considered simulated vineyards in Figs. 5b and 5c).

3.2. Relevance of using a spatial calibration approach

In Fig. 6, the more positive the ΔSBA value, the more the spatial calibration approach was relevant compared to an aspatial calibration at field or site-specific scale. The ΔSBA dispersion was different for both dates with high and low σ_Ψ. The variability of ΔSBA was higher for the date with a high σ_Ψ (August 18th). The results of Tukey's test (indicated by a letter on the top of the Figure) identify any significant differences between different combinations of spatial structure and ancillary data correlation. For both dates, ΔSBA were higher when ϱ_{AD} was higher, except for vineyards with weak spatial structures where the results were less contrasted, i.e. whatever the ϱ_{AD}, the difference in performance between aspatial and spatial calibration are similar. For moderate and strong SS_Ψ, increasing ϱ_{AD} increased significantly the relevance of using a spatial calibration approach. Using ϱ_{AD} at 94 % for these SS_Ψ modalities showed significant relevance of using spatial calibration whatever the σ_Ψ of the data. The violin plots (Fig. 6) showed that most of the ΔSBA values were relatively well grouped for all combinations of spatial structure and ancillary data correlations, but most did present some outliers.

Fig. 7 summarizes the effectiveness of spatial calibration compared to aspatial calibration. For a high σ_Ψ, spatial calibration was highly effective compared to site-specific aspatial calibration (i.e. ΔSBA_{site} positive) when SS_Ψ was strong with ϱ_{AD} was 94 %. However, its relevance decreased as ϱ_{AD} dropped, with performances at 50 % and 10 % ϱ_{AD} showing no improvement or even deterioration. For moderate or weak SS_Ψ, spatial calibration was generally not effective at the site-specific scale, with no significant advantages over aspatial calibration. Compared to an aspatial calibration at the field scale, spatial calibration performed well when SS_Ψ was strong or moderate with ϱ_{AD} at 94 %. At lower ϱ_{AD} (50 % and 10 %), performance tended to decline, especially for moderate SS_Ψ. When SS_Ψ was weak, spatial calibration provided no significant improvement, except for ϱ_{AD} at 10 %, which showed a slight decrease in accuracy.

For a low σ_Ψ, spatial calibration was effective when SS_Ψ was strong with ϱ_{AD} was 94 % (Fig. 7). However, for ϱ_{AD} at 50 % and 10 % with strong SS_Ψ, and for moderate SS_Ψ with ϱ_{AD} at 10 %, spatial calibration tended to reduce modeling performance. In other cases, the ΔSBA_{site} showed similar performances for spatial and aspatial calibration at the site-specific scale. For the ΔSBA_{field}, spatial calibration was effective with strong and moderate SS_Ψ with ϱ_{AD} of 94 %. In all other cases comparing to an aspatial calibration at the field scale, performances were better with spatial calibration. Overall, results for low σ_Ψ were less variable compared to those for high σ_Ψ.

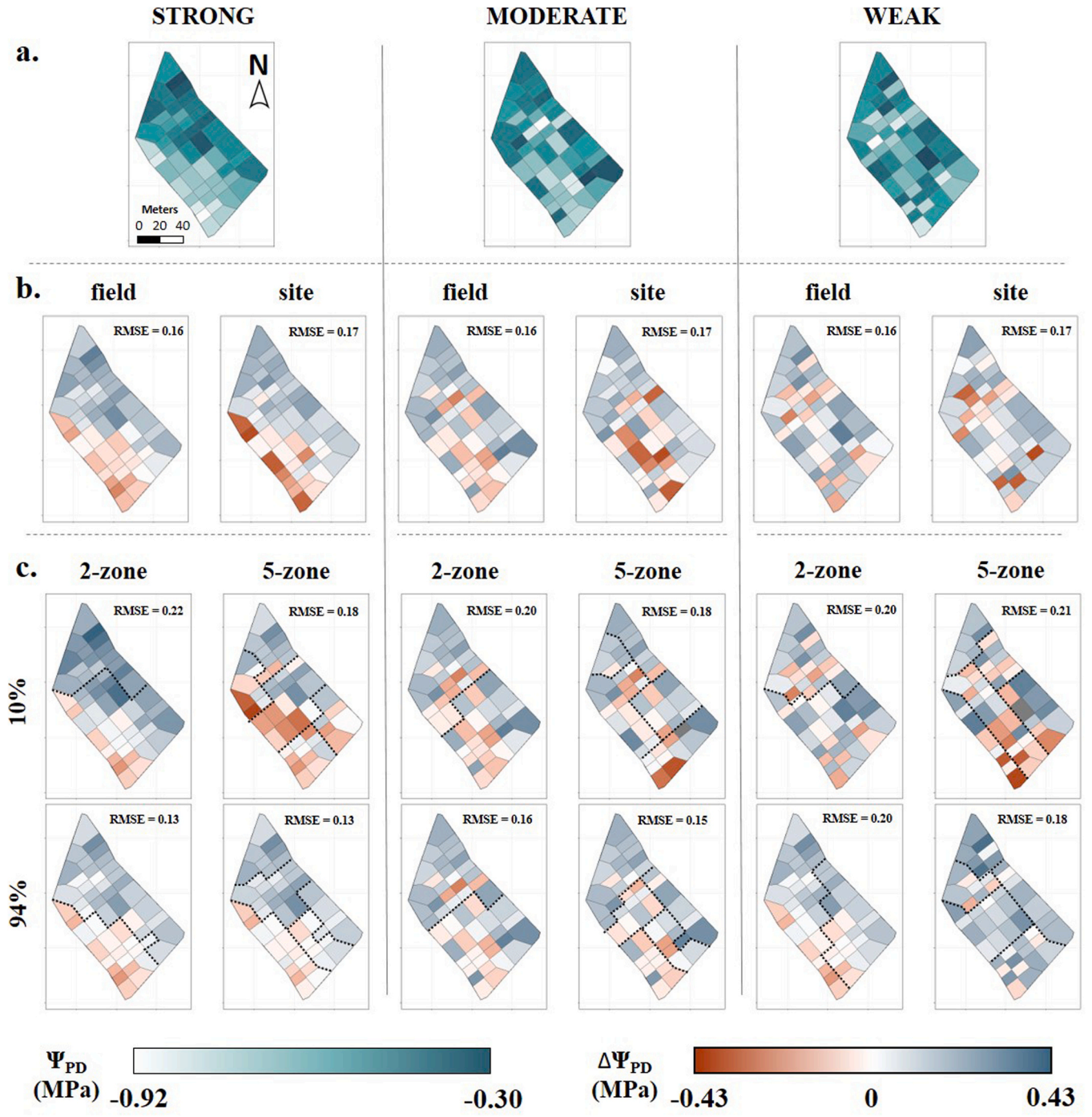

Fig. 5. Performances of WaLIS in predicting predawn leaf water potential (Ψ_{PD}) regarding each considered spatial structure of Ψ_{PD} (strong, moderate and weak) between the (a.) observed (simulated) Ψ_{PD} and modeling at different spatial scales: (b.) field and site-specific scale, (c.) at within-field scale (2-zone and 5-zone scales) for different level of correlation between Ψ_{PD} and the simulated ancillary data (10 % and 94 %). The presented modeling date were based on August 18th with a high Ψ_{PD} variability. Results are only shown for one simulated vineyard for each spatial structure modality. The dotted lines correspond to the delineated within-field zones for the considered simulated vineyard.

4. Discussion

4.1. Spatial calibration performances compared to field and site-specific scale calibration

Spatial calibration generally outperformed aspatial calibration at the field scale, particularly with high σ_Ψ (Fig. 7), as it better captured within-field variability. Similar results have been reported in recent studies (He et al., 2024; Trenz et al., 2024). However, field-scale calibration performed better for low σ_Ψ due to the low heterogeneity of the agronomic variable, which field-level data sufficiently represented. This aligns with the original design of crop growth models (CGM) for homogeneous field-scale areas. Compared to site-specific calibration, spatial calibration generally underperformed unless SS_Ψ was strong and ancillary data had a high ϱ_{AD} (Fig. 7). Site-specific calibration treats each site independently, ignoring spatial relationships, which can limit its effectiveness for variables with within-field heterogeneity. Similar results were already observed in other studies

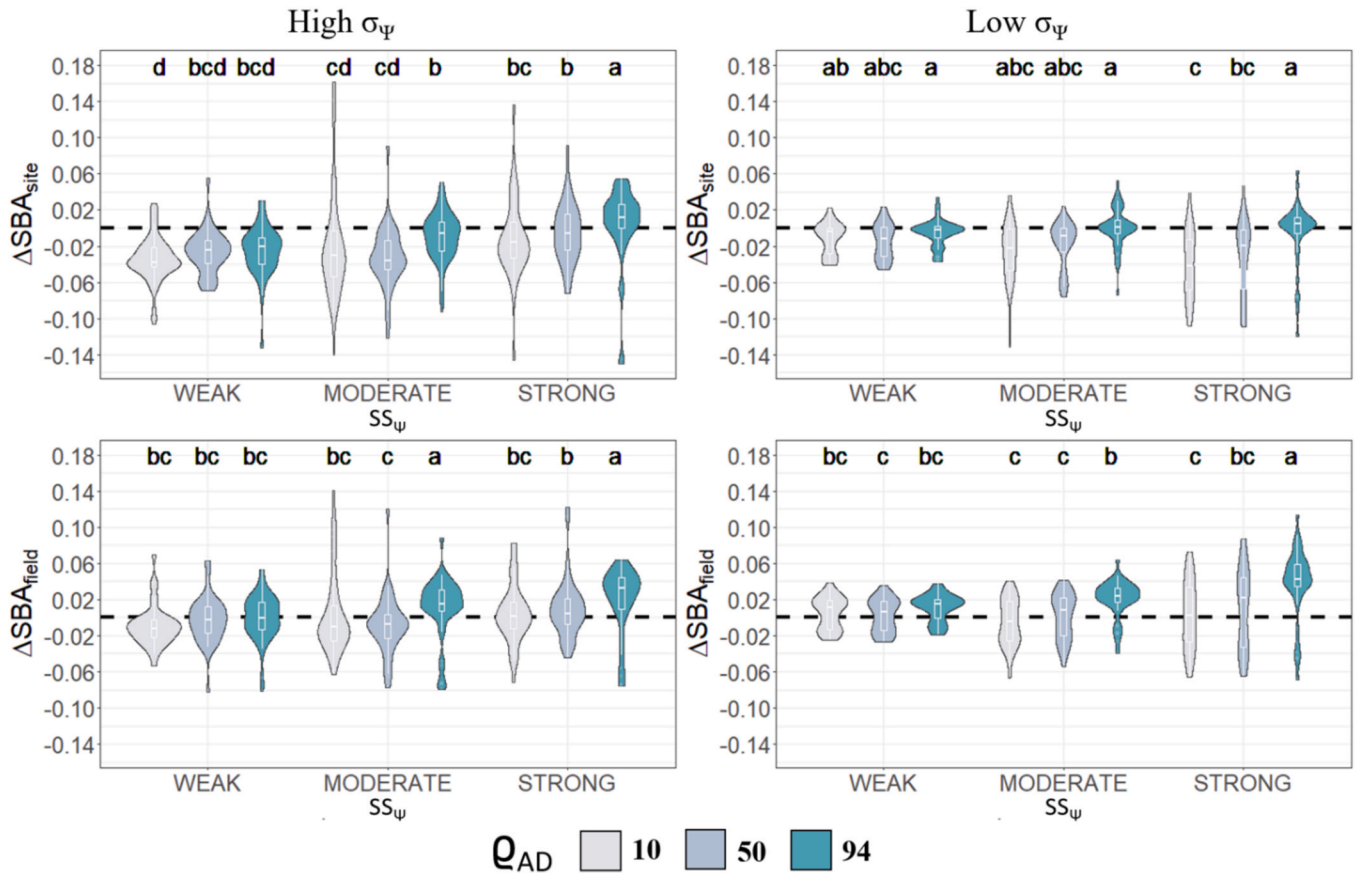

Fig. 6. Change in the SBA distributions using a spatial calibration approach compared to an aspatial calibration approach (at field scale at the bottom and at site-specific scale on top) depending on the spatial structure of the agronomic variable (SS_Ψ) (strong, moderate or weak), the variability of the agronomic variable (σ_Ψ) (high variability on right and low variability on left) and the correlation between the agronomic variable and the ancillary data (ϱ_{AD}) (Pearson's correlation of 10 %, 50 % and 94 %). A positive ΔSBA corresponds to better results with a spatial calibration approach, respectively a negative ΔSBA corresponds to a better result with aspatial calibration approach. Letters on the top are based on Tukey's test of significance. Modalities with the same letters are not significantly different at 0.05 probability level.

(Batchelor et al., 2002; He et al., 2024; Trenz et al., 2024). In cases of weak or moderate SS_Ψ, spatial calibration often deteriorated performances due to poorly defined calibration zones that introduced additional errors.

Previous studies already investigated using CGM at the within-field scale using either aggregated field data or site-specific measurements to calibrate the model (Batchelor et al., 2002; He et al., 2024; Thompson et al., 2024; Trenz et al., 2024). These studies mainly investigate if field or site-specific calibration better perform or if spatial calibration at the within-field scale could show better results. The innovation of this study lies in identifying conditions where spatial calibration is most effective and determining the optimal size of the specific unit (within-field zone). Here, the optimal size directly refers to the choice of whether or not to use spatial calibration. Indeed, adopting a spatial calibration approach involves the use of within-field calibration zones. Therefore, the trade-off between using an aspatial calibration (at the field or site-specific scale) and a spatial calibration approach (within-field calibration with 2–5 zones in this study) is directly related to the concept of optimal size. The optimal size is considered by computing the ΔSBA_{site} and ΔSBA_{field} between respectively the site-specific and the field scale with the optimal size within the within-field scale considered.

Even when spatial and aspatial calibration at the site-specific scale performed equally, spatial calibration offered the advantage of partially reproducing the spatial pattern of the agronomic variable. Furthermore, the most widely used CGM in crop modeling require dozens of input parameters. Using a spatial calibration approach, based on calibration zones, allows to reduce the number of parameters to calibrate and thus reduce the effort and time needed in the calibration processes. By incorporating spatial constraints into the calibration process, spatial calibration helped mitigate a part of the calibration error that occurred when ignoring the spatial pattern of the agronomic variable. Thus, a trade-off must be found between the level of model downscaling (within-field zone calibration) and the aggregation of available data used for spatial calibration at field scale. In this context, downscaling by creating management zones, and potentially multiple levels of zones, may offer an effective strategy for achieving accurate model calibration. When carefully applied, spatial calibration can preserve the spatial structure of the variable while minimizing the influence of stochastic error in the measured data used as calibration dataset and in the modeling process. This approach aimed to reduce calibration uncertainty, particularly for poor-quality, high-resolution data. However, considering the spatial structure is only beneficial in the favorable conditions outlined by this study.

4.2. Spatial calibration performance and availability of ancillary data

The effectiveness of spatial calibration decreased with a decreasing of ϱ_{AD}. It was most effective at high ϱ_{AD} (94 %), where the spatial patterns of the ancillary data and target variable closely aligned, allowing accurate delineation and significant performance improvements. At ϱ_{AD} of 50 %, commonly seen in agri-datasets, results varied and depended on the target variable variability. For very low correlations ($\varrho_{AD} = 10$ %), delineation failed to create meaningful zones, and spatial calibration performed worse than field or site-specific calibration. Only one single

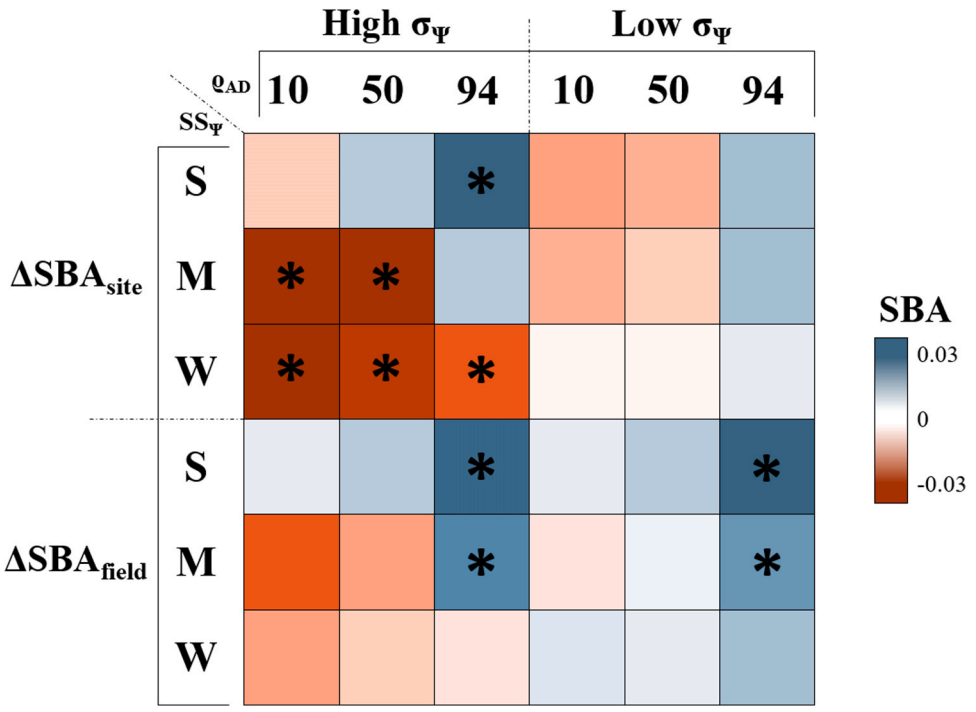

Fig. 7. Relevance of using a spatial calibration compared to an aspatial calibration regarding the difference of SBA score for different spatial scales of modelling. Significances were estimated with a Tukey test (modalities with different letters) and correspond to a significant improvement or deterioration of the spatialized crop model (represented by *). Blue cases correspond to a better performance of a spatial calibration compared to an aspatial calibration. Red cases correspond to a better performance of an aspatial calibration compared to a spatial calibration. σ_Ψ corresponds to the variability of Ψ_{PD}, S, M and W correspond to the spatial structure modalities SS_Ψ (respectively strong, moderate and weak), 10, 50 and 94 correspond to the ancillary data correlation ϱ_{AD} (respectively 10 %, 50 % and 94 %).

ancillary data layer was chosen for this study to simplify the assumptions and the simulation of the ancillary data used. In reality, for a relevant and reliable use of ancillary data, several types of data should be used to better describe the spatial pattern of the agronomic variable (Derby et al., 2007). Data fusion is necessary to integrate several sources of ancillary data (e.g. soil and plant data) to have a more accurate delineation of within-field zones (Castrignanò et al., 2019).

The aim of spatial calibration was to replicate the spatial pattern of the agronomic variable at a specific modeling date. This study assumed that the spatial patterns used to define within-field calibration zones remained static throughout the growing season and across production years. Similar assumptions have been adopted in other studies using static within-field zones (Hedley and Yule, 2009; Liu et al., 2018b; Stone et al., 2015). For the spatial calibration approach, the spatial pattern in the ancillary data must be available prior to the calibration process. Typically, such data are accessible at the beginning of the growing season, as they often originate from previous years, such as yield maps or relatively stable soil characteristics (e.g., soil texture, apparent soil electrical conductivity) (Nawar et al., 2017).

4.3. In-season dynamic within-field delineation

Spatial patterns, on which the calibration zones are assumed to be delineated, may be temporally dynamic for many agronomic traits (Anastasiou et al., 2019). Thus, spatial calibration might not account for changes over time within a growing season, as the within-field calibration zones are fixed at the beginning of the modeling process and then static. Here, delineation was based on a date where the Ψ_{PD} was the more spatially heterogeneous. However, spatial calibration based on static calibration zones can be not relevant in case of field with strong time dependency. Many studies already investigated the relevance of using dynamic within-field zones for irrigation management (Cohen et al., 2017; Evans et al., 2013; Zhang et al., 2024). Such approach needs to have a strong spatiotemporal resolution, which can be achieved using (low-cost) remote sensing data or sensors spread at within-field scale (Fontanet et al., 2020). However, using both kind of ancillary data with relatively stable spatial pattern characteristics (e.g. soil texture) and variables with changing spatial pattern from year to year depending on weather conditions (e.g. yield maps, crop coverage) has been identified as possible alternative to fully integrate the spatial pattern at the within-field scale (Nawar et al., 2017).

4.4. Spatial crop models: another spatialization process

Soil characteristics, and especially water fluxes, have a significant impact on CGM performances (Schmitter et al., 2015; Ward et al., 2018). However, CGM typically consider only vertical water fluxes, spatially constrained applications may integrate horizontal water fluxes by coupling CGM with hydrological models. Studies adopting this approach provide a more comprehensive representation of water dynamics (Huth et al., 2012; Shelia et al., 2018; Tenreiro et al., 2022; Xiang et al., 2020). Both input parameters considered to describe the within-field variability were related to the soil and the vine vigor. Climate data used were considered homogenous at the field level. However, microclimate in vineyard can have a huge impact on evapotranspiration and be heterogeneous at the row scale (Pereira et al., 2006; Torres et al., 2017). CGM are usually implemented with vertical water fluxes in the field. A more accurate representation of spatial interactions could be achieved by considering horizontal fluxes (e.g., runoff) to better capture within-field heterogeneity (Huth et al., 2012; Xiang et al., 2020).

5. Conclusion

This study examined the impact of spatial structure characteristics, total variance, and the level of correlation between an agronomic variable and ancillary data on the effectiveness of a spatial calibration approach. The findings demonstrated that spatial calibration significantly enhanced modeling performance when the agronomic variable

exhibited a strong spatial structure, a high variability, and a strong correlation with ancillary data used to delineate within-field zones (calibration zones). However, cases with moderate or weak spatial structure and high variability did not show similar benefits, highlighting the need for careful consideration of these conditions. For agronomic variables with low variability, no performance differences were observed between field or site-specific and spatial calibration approaches. This work provides new insights into spatializing CGM by downscaling predictions through the definition of within-field calibration zones. It advances understanding of how to increase the spatial resolution of crop models at the within-field scale, with the ultimate goal of improving agronomic practices to support more sustainable agriculture in a precision agriculture context.

CRediT authorship contribution statement

Bruno Tisseyre: Methodology, Validation, Conceptualization, Writing – review & editing. **Sébastien Roux:** Writing – review & editing, Investigation, Methodology, Conceptualization, Validation. **Daniel Pasquel:** Methodology, Formal analysis, Writing – original draft, Investigation, Writing – review & editing, Conceptualization. **James A. Taylor:** Conceptualization, Validation, Funding acquisition, Writing – review & editing, Methodology.

Declaration of Competing Interest

The authors declare that they have no known competing financial interests or personal relationships that could have appeared to influence the work reported in this paper.

Acknowledgements

This work was supported by the French National Research Agency under the Investments for the Future Program, referred as ANR-16-CONV-0004. This work has been realized with the support of MESO@LR-Platform at the University of Montpellier.

Appendix A. Supporting information

Supplementary data associated with this article can be found in the online version at doi:10.1016/j.eja.2025.127773.

Data availability

Data used in this study are available at this link: https://github.com/dpasquel/spatial_calibration_data

References

Acevedo-Opazo, C., Tisseyre, B., Guillaume, S., Ojeda, H., 2008. The potential of high spatial resolution information to define within-vineyard zones related to vine water status. Precis. Agric. 9 (5), 285–302. https://doi.org/10.1007/s11119-008-9073-1.

Acevedo-Opazo, C., Tisseyre, B., Taylor, J.A., Ojeda, H., Guillaume, S., 2010. A model for the spatial prediction of water status in vines (Vitis vinifera L.) using high resolution ancillary information. Precis. Agric. 11 (4), 358–378. https://doi.org/10.1007/s11119-010-9164-7.

Allen, R.G., Jensen, M.E., Wright, J.L., Burman, R.D., 1989. Operational Estimates of Reference Evapotranspiration. Agron. J. 81 (4), 650–662. https://doi.org/10.2134/agronj1989.00021962008100040019x.

Anastasiou, E., Castrignanò, A., Arvanitis, K., Fountas, S., 2019. A multi-source data fusion approach to assess spatial-temporal variability and delineate homogeneous zones: A use case in a table grape vineyard in Greece. Sci. Total Environ. 684, 155–163. https://doi.org/10.1016/j.scitotenv.2019.05.324.

Bahat, I., Netzer, Y., Grünzweig, J.M., Naor, A., Alchanatis, V., Ben-Gal, A., Keisar, O., Lidor, G., Cohen, Y., 2024. How do spatial scale and seasonal factors affect thermal-based water status estimation and precision irrigation decisions in vineyards? Precis. Agric. 25 (3), 1477–1501. https://doi.org/10.1007/s11119-024-10120-5.

Batchelor, W.D., Basso, B., Paz, J.O., 2002. Examples of strategies to analyze spatial and temporal yield variability using crop models. Eur. J. Agron. 18 (1-2), 141–158. https://doi.org/10.1016/S1161-0301(02)00101-6.

Bramley, R.G.V., Ouzman, J., Trought, M.C.T., Neal, S.M., Bennett, J.S., 2019. Spatio-temporal variability in vine vigour and yield in a Marlborough Sauvignon Blanc vineyard. Aust. J. Grape Wine Res. 25 (4), 430–438. https://doi.org/10.1111/ajgw.12408.

Cambardella, C.A., Moorman, T.B., Novak, J.M., Parkin, T.B., Karlen, D.L., Turco, R.F., Konopka, A.E., 1994. Field-Scale Variability of Soil Properties in Central Iowa Soils. Soil Sci. Soc. Am. J. 58 (5), 1501–1511. https://doi.org/10.2136/sssaj1994.03615995005800050033x.

Cammarano, D., Basso, B., Holland, J., Gianinetti, A., Baronchelli, M., Ronga, D., 2021. Modeling spatial and temporal optimal N fertilizer rates to reduce nitrate leaching while improving grain yield and quality in malting barley. Comput. Electron. Agric. 182, 105997. https://doi.org/10.1016/j.compag.2021.105997.

Castrignanò, A., Quarto, R., Venezia, A., Buttafuoco, G., 2019. A comparison between mixed support kriging and block cokriging for modelling and combining spatial data with different support. Precis. Agric. 20 (2), 193–213. https://doi.org/10.1007/s11119-018-09630-w.

Celette, F., Ripoche, A., Gary, C., 2010. WaLIS—A simple model to simulate water partitioning in a crop association: The example of an intercropped vineyard. Agric. Water Manag. 97 (11), 1749–1759. https://doi.org/10.1016/j.agwat.2010.06.008.

Cohen, Y., Alchanatis, V., Saranga, Y., Rosenberg, O., Sela, E., Bosak, A., 2017. Mapping water status based on aerial thermal imagery: Comparison of methodologies for upscaling from a single leaf to commercial fields. Precis. Agric. 18 (5), 801–822. https://doi.org/10.1007/s11119-016-9484-3.

Corwin, D.L., Lesch, S.M., 2005. Apparent soil electrical conductivity measurements in agriculture. Comput. Electron. Agric. 46 (1-3), 11–43. https://doi.org/10.1016/j.compag.2004.10.005.

Delannoy, D., Maury, O., Décome, J., 2022. CLIMATIK Syst. ème D. 'Inf. pour Les. données du R. éseau agroclimatique INRAE (Version V1) [Jeu De. données]. https://doi.org/10.57745/AJNXEN.

Derby, N.E., Casey, F.X.M., Franzen, D.W., 2007. Comparison of Nitrogen Management Zone Delineation Methods for Corn Grain Yield. Agron. J. 99 (2), 405–414. https://doi.org/10.2134/agronj2006.0027.

Evans, R.G., LaRue, J., Stone, K.C., King, B.A., 2013. Adoption of site-specific variable rate sprinkler irrigation systems. Irrig. Sci. 31 (4), 871–887. https://doi.org/10.1007/s00271-012-0365-x.

Fontanet, M., Scudiero, E., Skaggs, T.H., Fernàndez-Garcia, D., Ferrer, F., Rodrigo, G., Bellvert, J., 2020. Dynamic Management Zones for Irrigation Scheduling. Agric. Water Manag. 238, 106207. https://doi.org/10.1016/j.agwat.2020.106207.

Gaso, D.V., De Wit, A., Berger, A.G., Kooistra, L., 2021. Predicting within-field soybean yield variability by coupling Sentinel-2 leaf area index with a crop growth model. *308-309* Agric. For. Meteorol., 108553. https://doi.org/10.1016/j.agrformet.2021.108553.

Guillaume, S., & Lablée, J.L. (2022). GeoFIS: Spatial Data Processing for Decision Making. R package version 1.0.3. <https://CRAN.R-project.org/package=GeoFIS>

Hall, A., Lamb, D.W., Holzapfel, B.P., Louis, J.P., 2011. Within-season temporal variation in correlations between vineyard canopy and winegrape composition and yield. Precis. Agric. 12 (1), 103–117. https://doi.org/10.1007/s11119-010-9159-4.

He, D., Wang, E., Kirkegaard, J., Han, E., Malone, B., Swan, T., Brown, S., Glover, M., Lawes, R., Lilley, J., 2024. Usefulness of techniques to measure and model crop growth and yield at different spatial scales. Field Crops Res. 309, 109332. https://doi.org/10.1016/j.fcr.2024.109332.

Hedley, C.B., Yule, I.J., 2009. Soil water status mapping and two variable-rate irrigation scenarios. Precis. Agric. 10 (4), 342–355. https://doi.org/10.1007/s11119-009-9119-z.

Huth, N.I., Bristow, K.L., Verburg, K., 2012. SWIM3: Model Use, Calibration, and Validation. Trans. ASABE 55 (4), 1303–1313. https://doi.org/10.13031/2013.42243.

Irmak, A., Jones, J.W., Batchelor, W.D., Paz, J.O., 2001. Estimating spatially variable soil properties for application of crop models in precision farming. Trans. ASAE 44 (5), 1343–1353. https://doi.org/10.13031/2013.6424.

Kerry, R., Oliver, M.A., 2007. Comparing sampling needs for variograms of soil properties computed by the method of moments and residual maximum likelihood. Geoderma 140 (4), 383–396. https://doi.org/10.1016/j.geoderma.2007.04.019.

Lebon, E., Dumas, V., Pieri, P., Schultz, H.R., 2003. Modelling the seasonal dynamics of the soil water balance of vineyards. Funct. Plant Biol. 30 (6), 699. https://doi.org/10.1071/FP02222.

Leo, S., De Antoni Migliorati, M., Nguyen, T.H., Grace, P.R., 2023. Combining remote sensing-derived management zones and an auto-calibrated crop simulation model to determine optimal nitrogen fertilizer rates. Agric. Syst. 205, 103559. https://doi.org/10.1016/j.agsy.2022.103559.

Liu, L., Wallach, D., Li, J., Liu, B., Zhang, L., Tang, L., Zhang, Y., Qiu, X., Cao, W., Zhu, Y., 2018a. Uncertainty in wheat phenology simulation induced by cultivar parameterization under climate warming. Eur. J. Agron. 94, 46–53. https://doi.org/10.1016/j.eja.2017.12.001.

Liu, H., Whiting, M.L., Ustin, S.L., Zarco-Tejada, P.J., Huffman, T., Zhang, X., 2018b. Maximizing the relationship of yield to site-specific management zones with object-oriented segmentation of hyperspectral images. Precis. Agric. 19 (2), 348–364. https://doi.org/10.1007/s11119-017-9521-x.

Maestrini, B., Basso, B., 2018. Predicting spatial patterns of within-field crop yield variability. Field Crops Res. 219, 106–112. https://doi.org/10.1016/j.fcr.2018.01.028.

McClymont, L., Goodwin, I., Whitfield, D.M., O'Connell, M.G., 2019. Effects of within-block canopy cover variability on water use efficiency of grapevines in the Sunraysia irrigation region, Australia. Agric. Water Manag. 211, 10–15. https://doi.org/10.1016/j.agwat.2018.09.028.

Nawar, S., Corstanje, R., Halcro, G., Mulla, D., Mouazen, A.M., 2017. Delineation of Soil Management Zones for Variable-Rate Fertilization. In: In Advances in Agronomy, 143. Elsevier, pp. 175–245. https://doi.org/10.1016/bs.agron.2017.01.003.

Oger, B., Vismara, P., Tisseyre, B., 2021. Combining target sampling with within field route-optimization to optimise on field yield estimation in viticulture. Precis. Agric. 22 (2), 432–451. https://doi.org/10.1007/s11119-020-09744-0.

van Oijen, M., Ewert, F., 1999. The effects of climatic variation in Europe on the yield response of spring wheat cv. Minaret to elevated CO2 and O3: An analysis of open-top chamber experiments by means of two crop growth simulation models. Eur. J. Agron. 10 (3), 249–264.

Pasquel, D., Cammarano, D., Roux, S., Castrignanò, A., Tisseyre, B., Rinaldi, M., Troccoli, A., Taylor, J.A., 2023. Downscaling the APSIM crop model for simulation at the within-field scale. Agric. Syst. 212, 103773. https://doi.org/10.1016/j.agsy.2023.103773.

Pasquel, D., Roux, S., Richetti, J., Cammarano, D., Tisseyre, B., Taylor, J.A., 2022. A review of methods to evaluate crop model performance at multiple and changing spatial scales. Precis. Agric. 23 (4), 1489–1513. https://doi.org/10.1007/s11119-022-09885-4.

Pasquel, D., Roux, S., Tisseyre, B., Taylor, J.A., 2023. A N. Metr. Eval. Spat. Crop Model Perform. 603–609. https://doi.org/10.3920/978-90-8686-947-3_76.

Pedroso, M., Taylor, J., Tisseyre, B., Charnomordic, B., Guillaume, S., 2010. A segmentation algorithm for the delineation of agricultural management zones. Comput. Electron. Agric. 70 (1), 199–208. https://doi.org/10.1016/j.compag.2009.10.007.

Pereira, G.E., Gaudillere, J.-P., Pieri, P., Hilbert, G., Maucourt, M., Deborde, C., Moing, A., Rolin, D., 2006. Microclimate Influence on Mineral and Metabolic Profiles of Grape Berries. J. Agric. Food Chem. 54 (18), 6765–6775. https://doi.org/10.1021/jf061013k.

Pereira, L.S., Perrier, A., Allen, R.G., Alves, I., 1999. Evapotranspiration: Concepts and Future Trends. J. Irrig. Drain. Eng. 125 (2), 45–51. https://doi.org/10.1061/(ASCE)0733-9437(1999)125:2(45).

R Core Team. (2023). R: A Language and Environment for Statistical Computing [Logiciel]. R Foundation for Statistical Computing. https://www.R-project.org/.

Roux, S., Gaudin, R., Tisseyre, B., 2019. Why does spatial extrapolation of the vine water status make sense? Insights from a modelling approach. Agric. Water Manag. 217, 255–264. https://doi.org/10.1016/j.agwat.2019.03.013.

Schmitter, P., Zwart, S.J., Danvi, A., Gbaguidi, F., 2015. Contributions of lateral flow and groundwater to the spatio-temporal variation of irrigated rice yields and water productivity in a West-African inland valley. Agric. Water Manag. 152, 286–298. https://doi.org/10.1016/j.agwat.2015.01.014.

Seidel, S.J., Palosuo, T., Thorburn, P., Wallach, D., 2018. Towards improved calibration of crop models – Where are we now and where should we go? Eur. J. Agron. 94, 25–35. https://doi.org/10.1016/j.eja.2018.01.006.

Shelia, V., Šimůnek, J., Boote, K., Hoogenbooom, G., 2018. Coupling DSSAT and HYDRUS-1D for simulations of soil water dynamics in the soil-plant-atmosphere system. J. Hydrol. Hydromech. 66 (2), 232–245. https://doi.org/10.1515/johh-2017-0055.

Stone, K.C., Bauer, P.J., Busscher, W.J., Millen, J.A., Evans, D.E., Strickland, E.E., 2015. Variable-rate irrigation management using an expert system in the eastern coastal plain. Irrig. Sci. 33 (3), 167–175. https://doi.org/10.1007/s00271-014-0457-x.

Tagarakis, A.C., Koundouras, S., Fountas, S., Gemtos, T., 2018. Evaluation of the use of LIDAR laser scanner to map pruning wood in vineyards and its potential for management zones delineation. Precis. Agric. 19 (2), 334–347. https://doi.org/10.1007/s11119-017-9519-4.

Tenreiro, T.R., Jeřábek, J., Gómez, J.A., Zumr, D., Martínez, G., García-Vila, M., Fereres, E., 2022. Simulating water lateral inflow and its contribution to spatial variations of rainfed wheat yields. Eur. J. Agron. 137, 126515. https://doi.org/10.1016/j.eja.2022.126515.

Thompson, L.J., Archontoulis, S.V., Puntel, L.A., 2024. Simulating within-field spatial and temporal corn yield response to nitrogen with APSIM model. Precis. Agric. 25 (5), 2421–2446. https://doi.org/10.1007/s11119-024-10178-1.

Thorp, K.R., DeJonge, K.C., Kaleita, A.L., Batchelor, W.D., Paz, J.O., 2008. Methodology for the use of DSSAT models for precision agriculture decision support. Comput. Electron. Agric. 64 (2), 276–285. https://doi.org/10.1016/j.compag.2008.05.022.

Torres, R., Ferrara, G., Soto, F., López, J.A., Sanchez, F., Mazzeo, A., Pérez-Pastor, A., Domingo, R., 2017. Effects of soil and climate in a table grape vineyard with cover crops. Irrigation management using sensors networks. Ciência e Técnica Vitivinícola 32 (1), 72–81. https://doi.org/10.1051/ctv/20173201072.

Trenz, J., Memic, E., Batchelor, W.D., Graeff-Hönninger, S., 2024. Generic optimization approach of soil hydraulic parameters for site-specific model applications. Precis. Agric. 25 (2), 654–680. https://doi.org/10.1007/s11119-023-10087-9.

Verdugo-Vásquez, N., Acevedo-Opazo, C., Valdés-Gómez, H., Pañitrur-De la Fuente, C., Ingram, B., García de Cortázar-Atauri, I., Tisseyre, B., 2022. Identification of main factors affecting the within-field spatial variability of grapevine phenology and total soluble solids accumulation: Towards the vineyard zoning using auxiliary information. Precis. Agric. 23 (1), 253–277. https://doi.org/10.1007/s11119-021-09836-5.

Wallach, D., 2011. Crop Model Calibration: A Statistical Perspective. Agron. J. 103 (4), 1144–1151. https://doi.org/10.2134/agronj2010.0432.

Wallach, D., Makowski, D., Jones, J.W., Brun, F., 2014. Working with dynamic crop models—Methods. tools and examples for agriculture and environment (2nd éd. Elsevier.

Wallach, D., Thorburn, P., Asseng, S., Challinor, A.J., Ewert, F., Jones, J.W., Rotter, R., Ruane, A., 2016. Estimating model prediction error: Should you treat predictions as fixed or random? Environ. Model. Softw. 84, 529–539. https://doi.org/10.1016/j.envsoft.2016.07.010.

Wallor, E., Kersebaum, K.-C., Ventrella, D., Bindi, M., Cammarano, D., Coucheney, E., Gaiser, T., Garofalo, P., Giglio, L., Giola, P., Hoffmann, M.P., Iocola, I., Lana, M., Lewan, E., Maharjan, G.R., Moriondo, M., Mula, L., Nendel, C., Pohankova, E., Trombi, G., 2018. The response of process-based agro-ecosystem models to within-field variability in site conditions. Field Crops Res. 228, 1–19. https://doi.org/10.1016/j.fcr.2018.08.021.

Ward, N.K., Maureira, F., Stöckle, C.O., Brooks, E.S., Painter, K.M., Yourek, M.A., Gasch, C.K., 2018. Simulating field-scale variability and precision management with a 3D hydrologic cropping systems model. Precis. Agric. 19 (2), 293–313. https://doi.org/10.1007/s11119-017-9517-6.

Xiang, Z., Bailey, R.T., Nozari, S., Husain, Z., Kisekka, I., Sharda, V., Gowda, P., 2020. DSSAT-MODFLOW: A new modeling framework for exploring groundwater conservation strategies in irrigated areas. Agric. Water Manag. 232, 106033. https://doi.org/10.1016/j.agwat.2020.106033.

Zhang, M., Zhao, W., Zhu, C., Li, J., 2024. Influence of the sampling time interval of canopy temperature on the dynamic zoning of variable rate irrigation. Agric. Water Manag. 295, 108754. https://doi.org/10.1016/j.agwat.2024.108754.

Ziliani, M.G., Altaf, M.U., Aragon, B., Houborg, R., Franz, T.E., Lu, Y., Sheffield, J., Hoteit, I., McCabe, M.F., 2022. Early season prediction of within-field crop yield variability by assimilating CubeSat data into a crop model. Agric. For. Meteorol. 313, 108736. https://doi.org/10.1016/j.agrformet.2021.108736.